Journal of Materials Chemistry B

PAPER

View Article Online
View Journal

Published on 14 October 2016. Downloaded by Boston University on 06/11/2016 08:01:31.

Cite this: DOI: 10.1039/c6tb01674j

A synthetic bridging patch of modified co-electrospun dual nano-scaffolds for massive rotator cuff tear

Yaying Sun,†[a] Fei Han,†[b] Peng Zhang,[c] Yunlong Zhi,[a] Jianjun Yang,[c] Xiaohan Yao,[d] Hui Wang,[d] Chao Lin,[b] Xuejun Wen,[be] Jiwu Chen*[a] and Peng Zhao*[b]

Massive rotator cuff tears (MRCTs) are difficult to repair because of the retraction and poor mobility of torn tendons. In the current study, co-electrospun dual nano-scaffolds of poly(lactic-*co*-glycolic acid)/collagen I-polycaprolactone/nanohydroxyapatite (PLGA/Col-PCL/nHA) were fabricated and used to bridge MRCTs of infraspinatus tendons in a rabbit model. PLGA–PCL served as a control. The PLGA or the PLGA/Col sides of the dual scaffolds connected the tendon stumps. The PCL or PCL/nHA side was inserted into the bone tunnel at the insertion of the infraspinatus tendon. Fibroblasts showed higher viability and collagen secretion when seeded on a PLGA/Col scaffold compared to a PLGA scaffold. Osteoblasts seeded on a PCL/nHA scaffold grew better with higher mineralization than on a PCL scaffold. Histologically, collagen regenerated along PLGA scaffolds, but showed poor ingrowth to scaffolds compared with the PLGA/Col group. Newly formed bone was observed on the PCL scaffold, but was less than that on the PCL/nHA scaffold. At 6 weeks post repair, the regenerated tendon in both groups had similar maximum load to failure and ultimate stress but significantly lower stiffness in the PLGA–PCL group and a higher cross-sectional area in the PLGA/Col-PCL/nHA group compared with normal values. At 12 weeks, the maximum failure load, ultimate stress and cross-sectional areas of the regenerated tendon in the PLGA/Col-PCL/nHA group were significantly higher than in the PLGA–PCL and normal groups. The biomechanical properties of the PLGA–PCL group were similar to normal except for a larger cross-sectional area. Our data showed that the co-electrospun dual nano-scaffolds are promising in bridging MRCTs. Doping with Col and nHA further strengthens tissue regeneration.

Received 6th July 2016,
Accepted 13th October 2016

DOI: 10.1039/c6tb01674j

www.rsc.org/MaterialsB

Introduction

Rotator cuff tear is a common disorder with a prevalence ranging from 30% to 50% in patients older than 50 years old.[1] A complete tear with a diameter of more than 5 cm or of more than two tendons is defined as a massive rotator cuff tear (MRCT).[2,3] MRCTs are not uncommon, they constitute about 40% of all rotator cuff tears and present challenges for orthopedic surgeons to repair because of the retraction and poor mobility of the torn tendon.[4] Additionally, even if tendon–bone attachment is attained, MRCT has higher re-tear rate compared to smaller tears.[5–7]

To reduce tension and improve healing, bioabsorbable materials have been studied to bridge defects. Polyglycolic acid and poly-L-lactate-epsilon-caprolactone sheets have shown potential in repairing MRCTs.[8,9] Recently, electrospinning techniques have been employed to produce scaffolds for artificial grafts. Electrospun nano-scaffolds made from polymeric compounds are promising modalities in the promotion of tissue growth due to their good biocompatibility, high aspect ratios, and high porosity with small pore sizes.[10–12]

Among various polymers for electrospinning, polycaprolactone (PCL) and poly(lactide-*co*-glycolide) (PLGA) have been widely studied.[13–16] With its adjustable biodegradability, PCL was approved by the US Food and Drug Administration as a component of biomaterial-based scaffolds and has been proven to be a suitable material especially in bone tissue engineering.[17]

[a] *Department of Sports Medicine, Huashan Hospital, Fudan University, 12 Middle Wulumuqi Road, Shanghai, 200040, People's Republic of China. E-mail: jeevechen@gmail.com; Fax: +86 21 6249 6020; Tel: +86 21 5288 8255*
[b] *Shanghai East Hospital, The Institute for Biomedical Engineering and Nanoscience, Tongji University School of Medicine, Tongji University, Shanghai, 200040, People's Republic of China. E-mail: zp@tongji.edu.cn*
[c] *Department of Orthopedics, Shanghai Tenth People's Hospital, Tongji University School of Medicine, Shanghai, 200040, People's Republic of China*
[d] *Institute for Nutritional Sciences, Shanghai Institutes for Biological Sciences, Chinese Academy of Sciences, Shanghai, 200040, People's Republic of China*
[e] *Institute for Engineering and Medicine, Department of Chemical and Life Science Engineering, Virginia Commonwealth University, Richmond, Virginia 23284-3028, USA*
† These authors contributed equally to this work.

Published on 14 October 2016. Downloaded by Boston University on 06/11/2016 08:01:31.

Biodegradable and biocompatible PLGA is a popular material for tendon engineering because of its strong mechanical properties,[18,19] and it has already been proven to be able to augment repaired rotator cuffs compared with direct fixation.[20]

In order to enhance the biocompatibility of materials, a promising method is to mimic the natural micro-environment using a synthetic extracellular matrix (ECM).[21] Nanohydroxyapatite (nHA) is frequently used in bone engineering due to its physico-chemical features similar to those of natural nanocrystals in bone tissue.[22–24] Chen *et al.* found that a nano-scaffold made from PCL and nHA promotes the proliferation and osteogenic differentiation of mesenchymal stem cells.[25] As a major extracellular matrix (ECM) component, collagen I (Col) has the ability to promote cell growth, migration, and differentiation through interactions with growth factors, and enhance the biocompatibility of polymers.[26] A combination of both materials allows for better biocompatibility and overcomes the poor mechanical properties of Col.

Presently, the development of a single type of scaffold has been proven to be a primary success in repairing rotator cuff models.[27,28] However, the two sides of the tear are tendon and bone, which possess different anatomical, histological, and biomechanical characteristics. Therefore, there is increasing demand for a scaffold which can simultaneously promote bone-to-scaffold ingrowth as well as tendon-to-scaffold ingrowth. In order to balance tissue divergence, the idea of a co-electrospun dual nano-scaffold has been introduced into practice.[29]

In the current study, we made two types of co-electrospun dual nanoscaffolds, poly(lactic-*co*-glycolic acid)–polycaprolactone (PLGA–PCL) and poly(lactic-*co*-glycolic acid)/collagen I-polycaprolactone/nanohydroxyapatite (PLGA/Col-PCL/nHA), to bridge MRCTs in rabbit models. The PLGA or PLGA/Col side is used to connect the tendon stump, while the PCL or the PCL/nHA part is used to stimulate bone growth. Our hypothesis is that incorporation of Col and nHA on the dual scaffolds will have potential benefits for different tissue ingrowth in bridging the MRCTs.

Methods

Material preparation

PLGA (0.3 g) and Col (0.1 g) (both from Sigma-Aldrich Co., St Louis, MO, USA) were dissolved and stirred gently in 4.7 g hexafluoroisopropanol. After one-hour of stirring at 300 rotations per min, both materials were absolutely dissolved in solution. The ratio of PLGA was 6% in this mixed solvent. nHA and hexafluoroisopropanol were obtained from Aladdin (Shanghai, China). nHA (0.15 g) was first added into hexafluoroisopropanol (4.7 g) and kept dispersed by ultrasound. Then, PCL (0.3 g) (Sigma-Aldrich Co., St Louis, MO, USA) was dissolved in the mixed solution with a ratio of 6%. The ratio of nHA in the electrospun nano-scaffold of PCL/nHA was 33.3%.

The electrospun nanofiber was fabricated according to the previous method.[15] Briefly, the nanofiber, which was generated at a voltage of 15 kV (ZS-60 kV/2 mA, Rixing Electric Inc. Shanghai, People's Republic of China), was collected on an aluminum foil plate, 20 cm away from the solution delivery needle. Fabrication of the two-segment nanofibers was achieved with the assistance of a plastic plate half-covered by aluminum foil to ensure that the fibers only adhere to half of the foil. Six nanofiber scaffolds, *i.e.*, a PLGA scaffold, PLGA/Col scaffold, PCL scaffold, PCL/nHA scaffold, co-electrospun dual PLGA–PCL scaffold, and co-electrospun dual PLGA/Col-PCL/nHA scaffold were fabricated. The border between PLGA and PCL, PLGA/Col and PCL/nHA was marked on the aluminum foil plate.

Characterization

Scanning electron microscope analysis. The PCL group, PCL/nHA group, PLGA group, and PLGA/Col group specimens were observed using a scanning electron microscope (SEM) (Vega3, Tescan Co. Ltd, Brno, Czech Republic). The samples, vacuum coated with gold, were placed in the vacuum chamber of the electron microscope, and viewed at an accelerating voltage of 20 kV. The diameter of the fiber was measured using Image J software (TS5136MM, Tescan Co. Ltd, Seoul, South Korea).

Elementary composition analysis. The chemical composition of the nanofibers was analyzed using an energy dispersive spectrometer (EDS), and an attenuated total reflection Fourier-transform infrared meter (Tensor 27, Bruker, Woodlands, TX, USA) over a wavelength range of 4000 and 400 cm^{-1}.

Osteoblast and fibroblast culture. Murine NIH3T3 fibroblast cell lines and MC3T3 osteoblast cell lines were purchased from the Type Culture Collection of the Chinese Academy of Sciences (Shanghai, China) and the Chinese Academy of Sciences (Shanghai, China), respectively. The four nanofibers collected in aluminum foil, *i.e.*, PLGA fibers, PLGA/Col fibers, PCL fibers, and PCL/nHA fibers, were separately soaked in 75% ethanol for 30 minutes in culture dishes, and then cut into wafers with a diameter of 1.2 cm. After removing ethanol, the wafers were dried for 3 hours at room temperature and then adhered into each well of a 24-well plate using rat-tail collagen. Then the wafer was disinfected using ultraviolet light for 30 minutes. After washing with sterile phosphate-buffered saline (PBS) twice, NIH3T3 cells (10^4 cells per well) and MC3T3 cells (10^4 cells per well) were seeded on Dulbecco's Modified Eagle's Medium (DMEM) containing 10% fetal bovine serum (Gibco, Thermo Fisher Scientific, Waltham, MA, USA) as well as 1% penicillin and streptomycin solution (Gibco, Thermo Fisher Scientific, Waltham, MA, USA).

Cell morphology. In accordance with the method mentioned above, NIH3T3 cells and MC3T3 cells were cultured for 1, 2 and 3 days. For observation, they were washed twice with PBS and immersed in PBS containing 2.5% glutaraldehyde for 4 hours. The cells were then dehydrated in ethanol solution at concentrations of 30%, 50%, 70%, 80%, 90%, 95% and 100% and eventually dried at 25 °C. The samples were then gold-coated under vacuum and visualized using SEM (Vega3, Tescan Co. Ltd, Brno, Czech Republic).

Cell viability assay. The NIH3T3 cells (10^4 per well) were seeded in PLGA and PLGA/Col membranes, and the MC3T3 cells (10^4 per well) were seeded in PCL and PCL/nHA membranes, in the wells of a 24-well plate. Each of the four groups had three samples.

This journal is © The Royal Society of Chemistry 2016

Published on 14 October 2016. Downloaded by Boston University on 06/11/2016 08:01:31.

After culturing for 1, 2 and 3 days, a fluorescence-based live/dead assay was used to show cell viability. Simultaneous use of two fluorescent dyes allowed a two-color differentiation of live cells from the dead-cell population. At the conclusion of the 1, 2, and 3 day culture periods, live and dead cells were observed using a LIVE/DEAD Viability/Cytotoxicity Kit (KeyGEN Biotech, Nanjing, Jiangsu, China) according to the manufacturer's instruction. A fluorescence microscope (Olympus Corporation, Tokyo, Japan) was used to capture images.

Cell viability was measured using a Cell Counting Kit-8 assay (KeyGEN Biotech, Nanjing, Jiangsu, China). In brief, after removing the culture medium and washing the cell-scaffold samples twice with PBS, the specimens were incubated at 37 °C for 2.5 hours with 5% CO_2. Then, 200 μL incubated solutions from each well were transferred to a 96-well plate, and 100 μL of incubated medium was transferred into a 96-well culture plate. The absorbance at 450 nm was recorded using a microplate reader (Victor X, PerkinElmer Inc., Waltham, MA, USA).

Collagen secretion. The synthesis of Col in the NIH3T3 cells on scaffolds was measured using a hydroxyproline hydrolysis test.[30] 1 mL MC3T3 cells (10^4 mL^{-1}) were seeded on PLGA and PLGA/Col scaffolds and cultured according to the prescribed method. At the conclusion of 5 and 10 days, cells on the membrane were collected after trypsinization. Then the synthesis of Col was measured using a hydroxyproline kit according to the instructions (Nanjing Jiancheng Bioengineering Institute, Nanjing, China). The results were determined using a spectrophotometer at 550 nm to quantify the optical density (OD), which was then converted into the content of Col with a factor of 7.46 μg Col to 1 μg hydroxyproline. In order to eliminate the influence of cell numbers, the collagen secretion of each well was normalized by dividing the OD value of CCK-8 cell viability.

Mineralization. The difference in the osteogenic effect of MC3T3 cells on PCL/nHA and PCL membranes was measured by alkaline phosphatase (ALP) staining. The content of ALP is a direct reflection of the osteogenesis activity of the osteoblasts. A higher content of ALP, which stains as a deep blue, suggests a stronger mineralization capacity of cells. 1 mL MC3T3 cells (10^4 mL^{-1}) were seeded onto scaffolds and cultured in DMEM for one day. Then the medium was supplemented with 10 mM *b*-glycerol phosphate (Sigma), 0.1 mM dexamethasone (Sigma), and 50 mg mL^{-1} ascorbic acid (Sigma). After culturing for 5 and 10 days, the alkaline phosphatase (ALP) activity was evaluated. Prior to ALP staining, DAPI was counterstained for 10 minutes at room temperature to show cellular nuclei. After showing the nuclei, ALP staining of the same region was captured. Three random regions (200 × 200 μm) were selected and input into Image J software (National Institutes of Health, Bethesda, MA, USA) to evaluate the grayscale value of blue according to the previously published method.[20] Briefly, the picture, opened with the software, was changed to 8-bit and then the mean grayscale value of the selected area was measured. As the value of black is 0 and white is 255, the lesser the value, the deeper the color.

Animal study design and surgical procedure. The animal study was approved by the Institutional Animal Care and Use Committee of Fudan University and was conducted according to the Guide for the Care and Use of Laboratory Animals of Fudan University. Twenty four adult New Zealand White rabbits (12 weeks old, 2.5 ± 0.3 kg) underwent an operative infraspinatus tendon reconstruction procedure on their left anterior limbs under strictly aseptic conditions. The rabbits were randomly divided into PLGA–PCL and PLGA/Col-PCL/nHA groups. Anesthesia was induced by the intravenous administration of 3% pentobarbital (30 mg kg^{-1} body weight). The animal was placed prone on the operating table. After skin preparation, the left anterior limb was disinfected after skin preparation incisions were made. After being exposed, a 10 mm length of the full-thickness native infraspinatus tendon was removed from the insertion sites by sharp dissection to mimic the MRCT.[8,9] Then, a bone tunnel with a diameter of 2.5 mm was created with 2.5 K-wire at the humeral footprint of the torn tendon with a direction parallel to the course of the native infraspinatus tendon.

Before the operation, the bridging patch was prepared. The dual nano-scaffold was folded along a vertical line from the PLGA side to PCL side and formed a patch with a size of approximately 40 mm (length) × 2.5 mm (width) × 2 mm (thickness) to match the cuff. The midline, the border between the two segments of the nanofibers, was marked. The PCL or the PCL/nHA side of the prepared patch was pulled across the bone tunnel until the midline of the scaffold was flush with the upper opening of the tunnel, and then fixed to adjacent tissue at the outlet with Ethicon 2-0 PDS*II sutures (Ethicon Inc., USA). With a length of 10 mm to bridge the tear, the distal part of the PLGA or the PLGA/Col side was sutured to the tendon stump using Ethicon 2-0 PDS*II sutures (Ethicon Inc., USA) (Fig. 1). After the tendon was reconstructed, the wound was closed in separate layers. The rabbits were kept in cages for free activities after the surgical procedure.[8,28]

Histological and mechanical evaluation. The animals were sacrificed at 6 and 12 weeks post-surgery to harvest tissue specimens for histological and biomechanical analyses. For the histological study, the harvested infraspinatus tendon–humeral

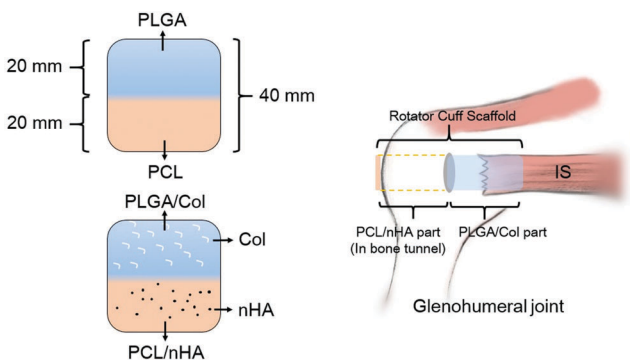

Fig. 1 Simulated image of the scaffolds and the fixation technique. The blue part wraps around the tendon stump and bridges the gap between the stump and the humerus. The orange part is crossed and fixed to the bone tunnel. Abbreviations: PLGA: poly(lactic-*co*-glycolic acid), PLGA/Col: poly(lactic-*co*-glycolic acid)/collagen I, PCL: polycaprolactone, PCL/nHA: polycaprolactone/nanohydroxyapatite, Col: collagen, nHA: nanohydroxyapatite, IS: infraspinatus tendon.

Published on 14 October 2016. Downloaded by Boston University on 06/11/2016 08:01:31.

head and shaft complex were fixed immediately in 10% neutral buffered formalin for 48 hours and were subsequently dehydrated through an alcohol gradient (30% to 100%), cleaned, and finally embedded in paraffin wax. The samples were sectioned perpendicularly to the longitudinal axis of the humerus tunnel with a thickness of 5 μm achieved by a microtome (SM2500; Leica Microsystems, Wetzlar Germany). The sections were stained with hematoxylin and eosin (HE) stain, Masson's trichrome stain, and Sirus red stain for histological evaluation. The graft-bone interface and the graft bridging the gap between the infraspinatus tendon and humerus were observed using inverted light microscopy (IX71SBF2; Olympus Corporation, Tokyo, Japan), with digital images taken using a DP72 Manager (Olympus Corporation, Japan). The amount of newly formed collagen, the width of the overlapping area between the scaffold and the newly formed collagen, and the area of the newly formed bone were quantified using image J (National Institutes of Health, Bethesda, MA, USA). The width of the overlapping and newly formed bone was measured from four randomly selected regions per picture from four histological pictures. The amount of newly formed tissue was calculated from four randomly selected areas (100 μm × 100 μm) per picture from four histological pictures by measuring the percentage of the area of newly formed tissue in the total selected area.[31]

For the mechanical study, a fresh specimen was tested using an electronic universal materials testing system machine (AGS-X, Shimadzu, Co., Kyoto, Japan) after harvest and preparation. Except for the artificial graft and the infraspinatus tendon, all muscle-tendon tissues were carefully removed. Prior to tensile testing, all samples were preloaded with a static preload of 1 N for 5 minutes, with the direction of force in line with the tunnel. After preconditioning, an ultimate failure load test was carried out with an elongation rate of 5 mm min^{-1}. The load–deformation curve was recorded, from which the maximal failure load (N) was measured. Stiffness at failure (N mm^{-1}) was calculated from the slope of the linear region of the load–deformation curve at the maximal load-to-failure point. To calculate the cross-sectional area (mm^2) of graft after surgery, the mean radius was measured using a vernier caliper with 0.1 mm in scale by measuring the radius of graft at 0 mm, 5 mm, and 10 mm away from the bony insertion. The stress (MPa) was calculated by maximum failure load/the cross-sectional area. These four values for the normal infraspinatus were also measured. The test was completed when the graft was broken or pulled out of the bone tunnel. The results were calculated from three independent samples.

Statistical analysis. All data were expressed as mean ± standard deviation. A Student's *t*-test was performed to detect statistically significant differences in the results of different experimental groups. Comparisons of groups at different time points were performed using an independent two-sample Student's *t*-test. For comparisons among multiple groups, one-way analysis of variance (ANOVA) and a post-hoc Tukey's test were performed. Statistical analysis was carried out using the SPSS Statistics 18.0 statistical software package, and a *P* value of less than 0.05 was considered statistically significant.

Results

Preparation and characteristics of nanofiber membrane

Fig. 2 shows an image of the nanofibers observed under SEM. PLGA nanofibers (570 ± 130 nm, Fig. 2A), PLGA/Col nanofibers (520 ± 120 nm, Fig. 2B), PCL nanofibers (530 ± 110 nm, Fig. 2C), and PCL/nHA nanofibers (550 ± 120 nm, Fig. 2D) were oriented randomly with a diameter comparable to each other without significant difference. In the image of the PCL/nHA nanofiber (Fig. 2D), small particles were observed. We suppose that it is a result of nHA aggregations. The element nitrogen was detected using EDS in the PLGA/Col nanofiber (Fig. 3B). Two peaks (K_α, and K_β, respectively) of the element calcium and a peak of phosphate were detected in the PCL/nHA nanofiber (Fig. 3D). FT-IR further showed that, at 1647 cm^{-1} and 1527 cm^{-1} in the

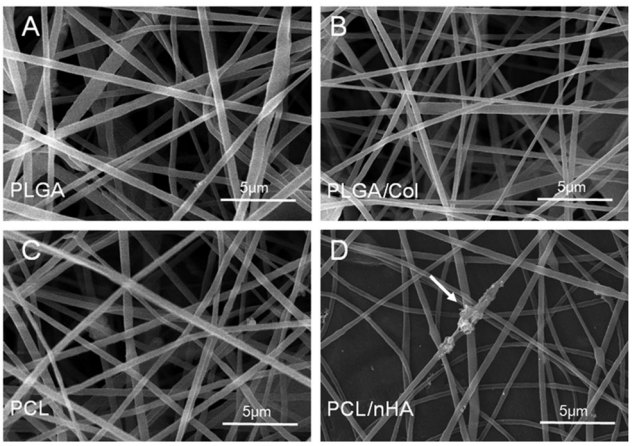

Fig. 2 The morphology of the different scaffolds viewed using a scanning electron microscope. The white arrow indicates nHA aggregations. Abbreviations: PLGA: poly(lactic-*co*-glycolic acid), PLGA/Col: poly(lactic-*co*-glycolic acid)/collagen I, PCL: polycaprolactone, PCL/nHA: polycaprolactone/nanohydroxyapatite.

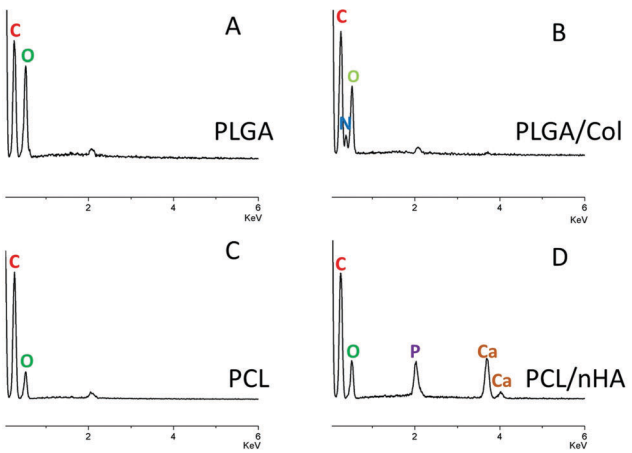

Fig. 3 Energy dispersive spectra showing the elements of the different scaffolds. Abbreviations: PLGA: poly(lactic-*co*-glycolic acid), PLGA/Col: poly(lactic-*co*-glycolic acid)/collagen I, PCL: polycaprolactone, PCL/nHA: polycaprolactone/nanohydroxyapatite, C: carbon, O: oxygen, N: nitrogen, P: phosphorus, Ca: calcium.

This journal is © The Royal Society of Chemistry 2016

Published on 14 October 2016. Downloaded by Boston University on 06/11/2016 08:01:31.

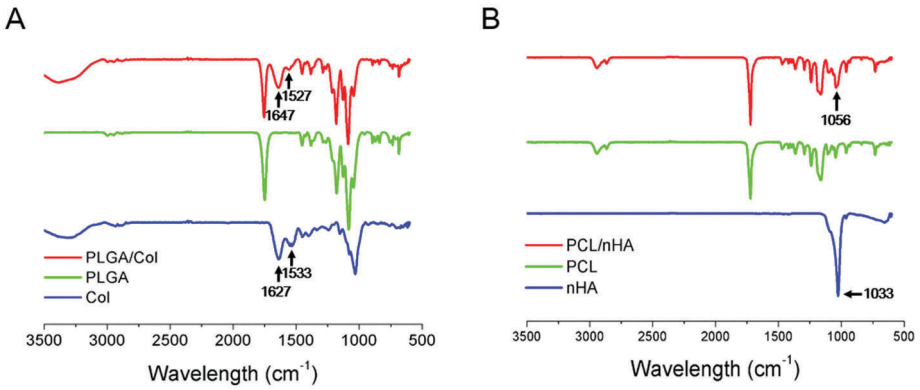

Fig. 4 Fourier-transform infrared spectra showing the elemental composition of the different scaffolds. Abbreviations: PLGA: poly(lactic-*co*-glycolic acid), PLGA/Col: poly(lactic-*co*-glycolic acid)/collagen I, Col: collagen I, PCL: polycaprolactone, PCL/nHA: polycaprolactone/nanohydroxyapatite, nHA: nanohydroxyapatite.

spectra of PLGA/Col rather than the PLGA nanofiber, two characteristic stretching bands of Col, an amide I band and an amide II band, were detected, supporting the incorporation of collagen (Fig. 4A). Compared with the PCL nanofiber, FT-IR validated the existence of nHA in the PCL/nHA nanofiber. A signal at 1056 cm^{-1}, indicating the presence of phosphate, was observed on the spectra of PCL/nHA rather than PCL, validating our hypothesis (Fig. 4B).

Cytocompatibility of electrospun membranes

SEM revealed that the NIH3T3 cells had good adhesion morphology with the PLGA and PLGA/Col membranes (Fig. 5), and the MC3T3 cells had good morphological characteristics with the PCL and PCL/nHA membranes (Fig. 6). After culturing for 1, 2, and 3 days, a fluorescence-based live/dead assay showed that the NIH3T3 and MC3T3 cells grew well on the scaffolds with almost no dead cells (Fig. 7). However, cell spreading was better on the scaffolds doped with Col or nHA compared to the simple scaffolds. CCK-8 assay further reported that for the NIH3T3 cells, cell viability was significantly higher on the PLGA/Col scaffold than on the PLGA scaffold after culturing for 3 days (Fig. 8A). Similarly, better MC3T3 viability was observed when cultured on the PCL/nHA scaffolds than on the PCL scaffolds (Fig. 8B). These results demonstrated that PLGA/Col provided a better environment for NIH3T3 growth than PLGA, and PCL/nHA was superior to PCL for osteoblast growth.

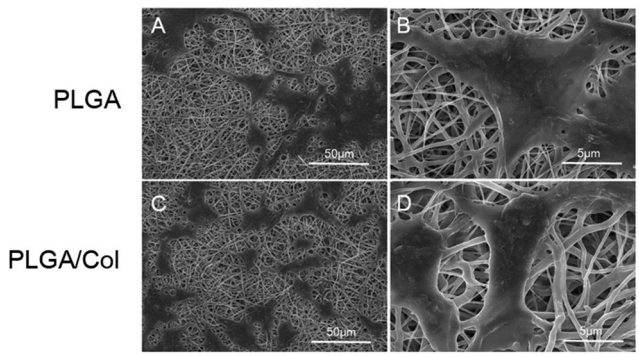

Fig. 5 NIH3T3 cell attachments on the scaffolds viewed using a scanning electron microscope. Abbreviations: PLGA: poly(lactic-*co*-glycolic acid), PLGA/Col: poly(lactic-*co*-glycolic acid)/collagen I.

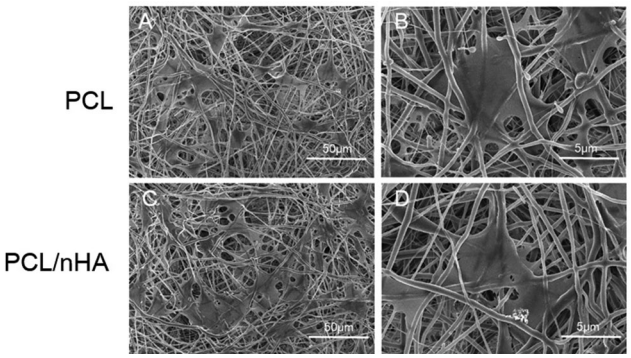

Fig. 6 MC3T3 cell attachments on the scaffolds viewed using a scanning electron microscope. Abbreviations: PCL: polycaprolactone, PCL/nHA: polycaprolactone/nanohydroxyapatite.

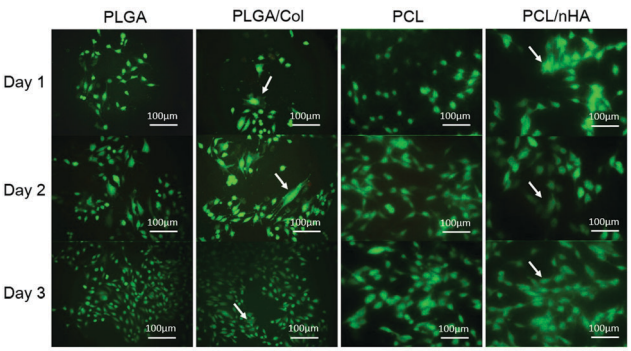

Fig. 7 Fluorescence-based live/dead assay showing the live and dead cells on different scaffolds with different culturing times. White arrows show cell spreading. Abbreviations: PLGA: poly(lactic-*co*-glycolic acid), PLGA/Col: poly(lactic-*co*-glycolic acid)/collagen I, PCL: polycaprolactone, PCL/nHA: polycaprolactone/nanohydroxyapatite.

Influence of electrospun membranes on collagen synthesis

After eliminating the effect of cell number, NIH3T3 cells cultured on PLGA/Col scaffolds secreted more Col, which was

Published on 14 October 2016. Downloaded by Boston University on 06/11/2016 08:01:31.

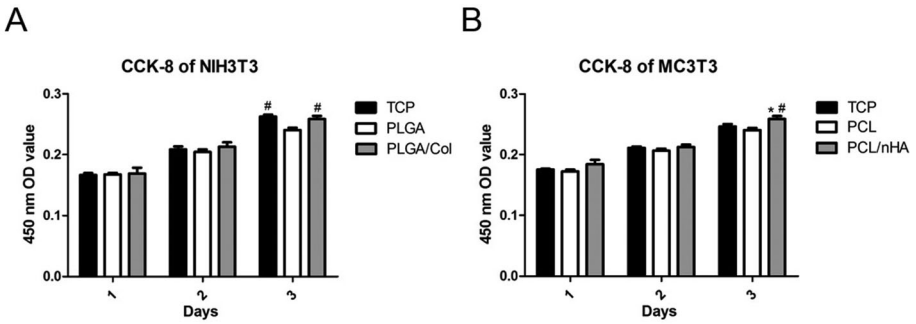

Fig. 8 The viability of cells on the different scaffolds. (A and B) The viability of fibroblasts (NIH3T3) and osteoblasts (MC3T3) on the scaffolds respectively, expressed as 450 nm optical density values. *$P < 0.05$ compared with normal values. #$P < 0.05$ compared with PCL/PLGA. Abbreviations: TCP: tissue culture plate, PLGA: poly(lactic-*co*-glycolic acid), PLGA/Col: poly(lactic-*co*-glycolic acid)/collagen I, PCL: polycaprolactone, PCL/nHA: polycaprolactone/nanohydroxyapatite.

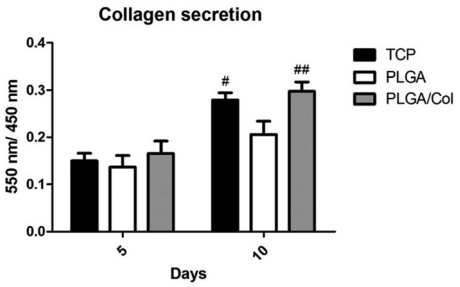

Fig. 9 The relative collagen secretion of fibroblasts (NIH3T3) on the different scaffolds after 5 and 10 days of culturing which was normalized to cell viability, expressed as 550 nm/450 nm optical density values. #$P < 0.05$ compared with PCL/PLGA. ##$P < 0.01$ compared with PCL/PLGA. Abbreviations: TCP: tissue culture plate, PLGA: poly(lactic-*co*-glycolic acid), PLGA/Col: poly(lactic-*co*-glycolic acid)/collagen I.

expressed as higher OD value compared with those cultured on PLGA scaffolds (Fig. 9). This outcome verified the superiority of PLGA/Col scaffolds over PLGA scaffolds in promoting fibroblast function.

Influence of electrospun membranes on osteogenesis

In the current study, ALP staining was different between the PCL and PCL/nHA scaffolds. Both at 5 days and 10 days after culture, deeper staining was observed in the samples in the PCL/nHA group than in the PCL group (Fig. 10.1). Using Image J software for a quantitative analysis, it was shown that, at the conclusion of 5 and 10 days after culture, the grayscale value of the PCL/nHA group was significantly lower than the PCL group ($P < 0.05$ and <0.01, respectively), manifesting the superiority of the PCL/nHA membrane in the augmentation of osteoblast cell mineralization (Fig. 10.2).

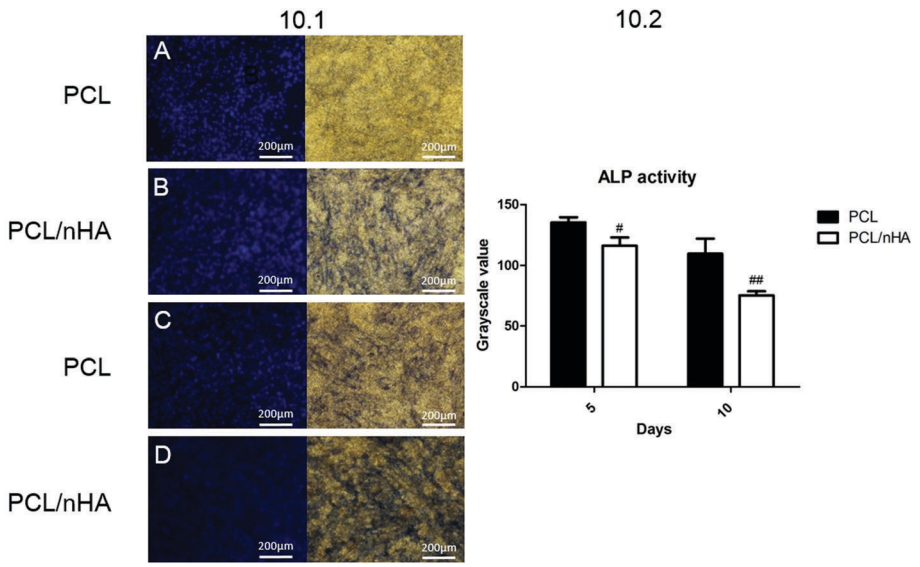

Fig. 10 The osteogenic activity of MC3T3 cells on different scaffolds expressed as the color of ALP stain (10.1) and quantitative analysis (10.2). In 10.1, the left column shows the DAPI stain, indicating the cells in the visual field, while the right column shows the ALP stain which indicates higher mineralization of MC3T3 in the PCL/nHA group (deeper blue) compared with the PCL group. A and B were captured at the conclusion of 5 days after culture, while C and D were captured at the conclusion of 10 days after culture. 10.2 shows the grayscale value of ALP staining of each group at each time point. Abbreviations: PCL: polycaprolactone, PCL/nHA: polycaprolactone/nanohydroxyapatite.

 This journal is © The Royal Society of Chemistry 2016

Published on 14 October 2016. Downloaded by Boston University on 06/11/2016 08:01:31.

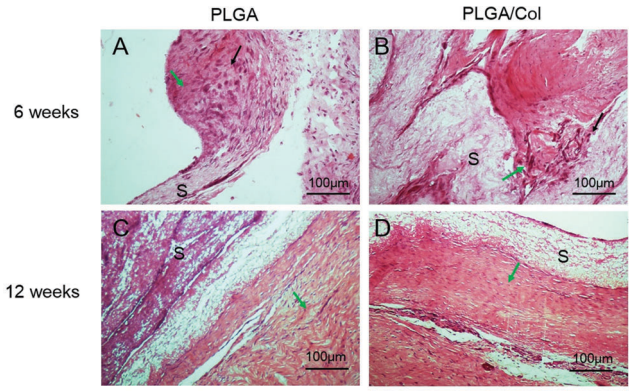

Fig. 11 Tissue regeneration of collagen on the different scaffolds at different time points *in vivo*, as shown using HE stain. Black arrows show inflammatory cell infiltration. Green arrows show newly formed collagen. Abbreviations: PLGA: poly(lactic-*co*-glycolic acid), PLGA/Col: poly(lactic-*co*-glycolic acid)/collagen I, S: scaffold.

Condition of subjects

Adhesion or contractures limiting the range of motion in the subjects was not observed. The scaffolds were visible and semi-opaque at the conclusion of 6 and 12 weeks after surgery. There was no infection at the surgical site in any of the specimens. No rupture of the scaffold-bridged tendons was noticed in any rabbits when sacrificed.

Histological findings

Inflammatory cells were observed at the end of the 6th week after surgery in the PLGA and PLGA/Col groups. Hardly any tendon-like tissue was observed in both groups (Fig. 11A and B). At the 12th week after surgery, the infiltration of inflammatory cells decreased and tendon-like tissue with regular fibers was observed in the PLGA/Col group rather than in the PLGA group (Fig. 11C and D). Using Sirus red stain, collagen secretion and arrangement was observed. At the 6th week, the collagen secreted on the PLGA/Col scaffolds was significantly denser than that on the PLGA scaffolds, while the width of the overlap between newly formed collagen and the scaffold in both groups was limited without significant difference (Fig. 12A–C). At the 12th week after surgery, the density of collagen attached on both scaffolds improved with no significant difference between the two groups. However, the width of the overlap between collagen and the scaffold were different. The overlap between newly formed collagen and the PLGA/Col scaffold was significantly wider than that between collagen and the PLGA scaffold at 12 weeks after surgery (Fig. 12D–F).

As shown in Fig. 13, at 6 weeks after surgery, the scaffold in the bone tunnel was observed with HE stain and inflammatory cells were infiltrated into the scaffold. Newly formed bone tissue was observed in the space within the folded scaffolds. At 12 weeks after surgery, the scaffold, although still present, had degenerated compared with the 6th week and the infiltration of inflammatory cells vanished. With Masson's staining, new bone

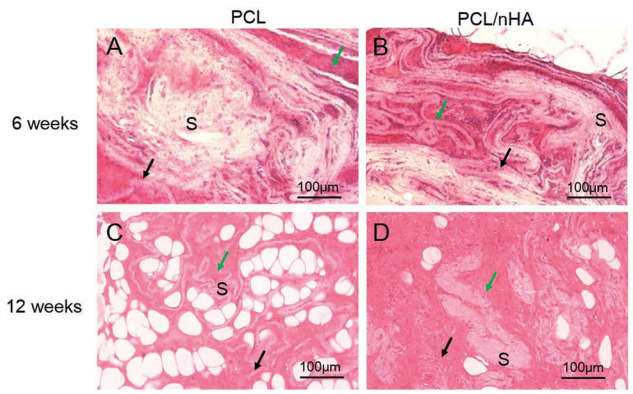

Fig. 13 Tissue regeneration of bone on the different scaffolds at different time points *in vivo*, as shown using HE stain. Black arrows show inflammatory cell infiltration. Green arrows show newly formed bone. Abbreviations: PCL: polycaprolactone, PCL/nHA: polycaprolactone/nanohydroxyapatite, S: scaffold.

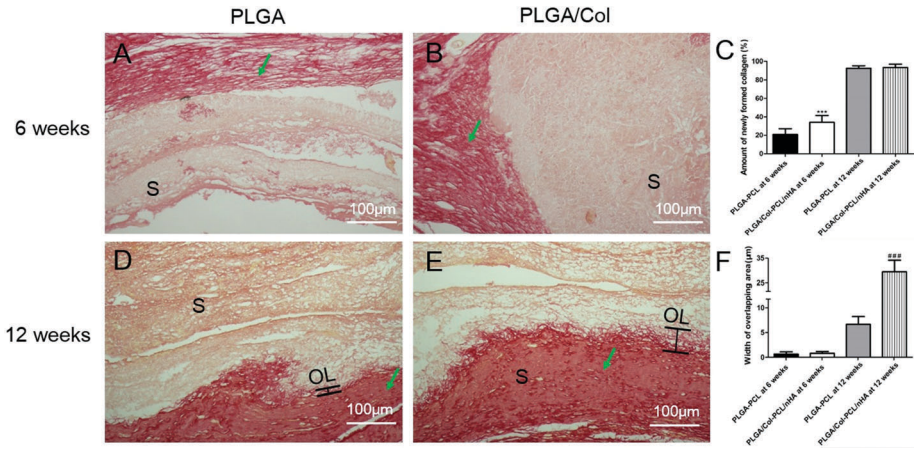

Fig. 12 Tissue regeneration of collagen on the different scaffolds at different time points *in vivo*, as shown using Sirus red stain (A and B are representative images of the collagen newly formed on PLGA and PLGA/Col scaffolds, respectively, while D and E are representative images of the collagen newly formed on PLGA and PLGA/Col scaffolds at 12 weeks, respectively). Green arrows show newly formed collagen. The amount of newly formed tendon and the width of the overlap between the newly formed tissues are quantified in C and F, respectively. Abbreviations: PLGA: poly(lactic-*co*-glycolic acid), PLGA/Col: poly(lactic-*co*-glycolic acid)/collagen I, OL: overlap, S: scaffold.

Published on 14 October 2016. Downloaded by Boston University on 06/11/2016 08:01:31.

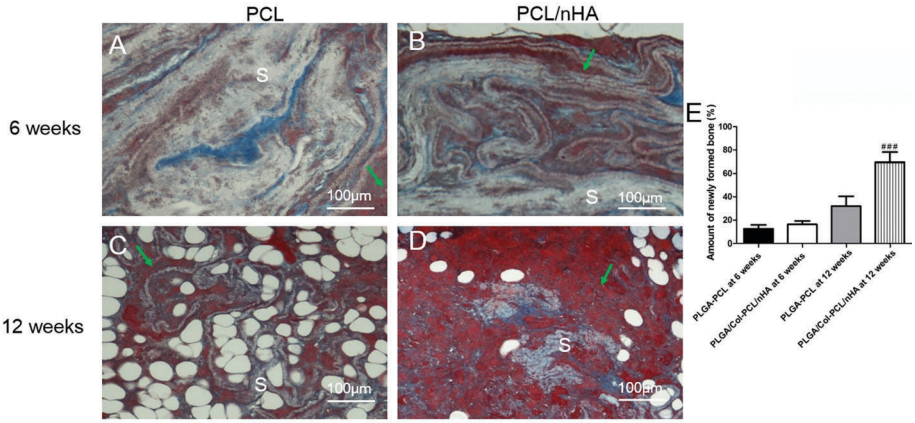

Fig. 14 Tissue regeneration of bone on the different scaffolds at different time points *in vivo*, as shown using Masson's stain (A and B are representative images of the bone newly formed on PCL and PCL/nHA scaffolds at 6 weeks, respectively, while C and D are representative images of the bone newly formed on PCL and PCL/nHA scaffolds at 12 weeks, respectively). The amount of newly formed bone is quantified in E. Green arrows show newly formed bone. Abbreviations: PCL: polycaprolactone, PCL/nHA: polycaprolactone/nanohydroxyapatite.

formation was observed as collagen stains. Compared with the PCL group, significantly more newly formed bone replaced the space of the dissolved PCL/nHA scaffold at 12 weeks but not 6 weeks after repair (Fig. 14).

Biomechanical testing

For normal infraspinatus–humerus complexes, the tendon is ruptured at the tendon–bone interface. For MRCTs repaired with scaffolds, no graft is pulled out from the tunnel at the end of the 6th week or 12th week after surgery. All surgically treated specimens were ruptured at or near the inlet of the bone tunnel.

As shown in Table 1, at the end of the 6th week after surgery, there was no difference among the PLGA/Col-PCL/nHA group, PLGA–PCL group, and normal values regarding maximum failure load and ultimate stress. However, the cross-sectional area of regenerated tendon in the PLGA/Col-PCL/nHA group was significantly higher than that in the PLGA–PCL group or the normal value, while the stiffness of the tendon in the PLGA–PCL group was significantly lower than that in the PLGA/Col-PCL/nHA group and the normal value. At the end of the 12th week after surgery, the tendon in the PLGA–PCL group and the normal value had similar maximum failure load and ultimate stress, but both values in both groups were significantly inferior to that of the PLGA/Col-PCL/nHA group. The tendon in the PLGA/Col-PCL/nHA group and the PLGA–PCL group had similar cross-sectional areas and were both significantly higher than the normal value. No difference was noted among the two scaffolds groups and the normal value in terms of tendon stiffness.

Discussion

A common problem in the repair of MRCTs is the high re-tear rate caused by excessive tension load on the repaired tendon and unstable healing at the tendon-to-bone insertion. Besides autografts and allografts, synthetic grafts with polymer augmentation systems have also been developed to repair MRCTs. Both clinical and laboratory studies have testified the application of synthesized membranes.[32–34] However, poor healing of tendon-grafts and bone-grafts is still a major concern. In recent years, electrospun nano-scaffolds have gained increasing interest because of the structure mimicking the extracellular matrix and the accessibility to various materials.[35] Therefore, to facilitate regeneration, the technology of electrospinning is a potential choice. With the use of PCL, PLGA, or other degenerative polymers with good bio-affinity, cells are able to adhere to and proliferate on the scaffold.

Previous studies have focused on single type electrospun membranes in rotator cuff repair. Inui *et al.*[28] verified that the

Table 1 Results of biomechanical tests

		6 weeks		12 weeks	
	Normal value	PLGA–PCL group	PLGA/Col-PCL/nHA group	PLGA–PCL group	PLGA/Col-PCL/nHA group
Maximum failure load	118.27 ± 8.41 N	112.13 ± 5.31 N	125.60 ± 11.95 N	136.10 ± 8.93 N	163.51 ± 11.32 N**#
Ultimate stress	22.81 ± 0.72 MPa	19.46 ± 1.99 MPa	21.28 ± 1.06 MPa	20.23 ± 1.77 MPa	24.32 ± 1.08 MPa#
Cross-sectional area	5.18 ± 0.21 mm^2	5.79 ± 0.39 mm^2	6.21 ± 0.25 mm^{2}*	6.39 ± 0.21 mm^{2}**	6.72 ± 0.36 mm^{2}**
Stiffness	21.16 ± 2.06 N mm^{-1}	15.71 ± 1.35 N mm^{-1}*	19.71 ± 1.99 N mm^{-1}	20.65 ± 2.22 N mm^{-1}	22.58 ± 1.92 N mm^{-1}

Abbreviations: PLGA: poly(lactic-*co*-glycolic acid), PLGA/Col: poly(lactic-*co*-glycolic acid)/collagen I, PCL: polycaprolactone, PCL/nHA: polycaprolactone/nanohydroxyapatite. *$P < 0.05$ compared with normal value. **$P < 0.01$ compared with normal value. #$P < 0.05$ compared with PCL/PLGA.

 This journal is © The Royal Society of Chemistry 2016

Published on 14 October 2016. Downloaded by Boston University on 06/11/2016 08:01:31.

poly(D,L-lactide-*co*-glycolide) (PLG) scaffold could be applied to bridge rotator cuff defects. The results showed that bridging with scaffolds can be equivalent to reattachment. Beason *et al.*[36] proved the validity of PCL electrospun scaffolds on a rat model of a supraspinatus tendon tear, while on the same rotator cuff tear model. Zhao *et al.*[20,37] found that PLLA or PLGA electrospun fibrous membranes had potential in promoting cell attachment and proliferation, as well as accelerating tendon-bone remodeling, and the loading of bFGF on PLGA further promotes enthesis healing.

In clinical practice, it is not uncommon to achieve healing between different tissues. In order to promote this process, co-electrospun dual nano-scaffolds which balance the different characteristics of tissues have been developed.[29,38] For the rotator cuff, an ideal scaffold should be able to promote bone-to-scaffold and tendon-to-scaffold ingrowth at two sides simultaneously. In the current study, a new type of nano-scaffold is testified in a MRCT model. For the purpose of mimicking the natural *in vivo* microenvironment, a co-electrospun dual nano-scaffold with PLGA and PCL was created. Furthermore, the Col and nHA were incorporated into PLGA fibers and PCL fibers respectively to improve biocompatibility.

Both *in vitro* and *in vivo*, the superiority of the PLGA/Col scaffold over PLGA was observed. Col has been proven to be able to enhance cellular migration in the formation of extracellular matrix and collagen secretion.[39] *In vivo*, fibroblasts on PLGA/Col had better viability and higher collagen secretion compared with PLGA. This advantage remained *in vivo*. In addition to the higher ultimate stress, the positive influence of Col on cell migration and collagen secretion was observed histologically. In PLGA/Col group, better collagen secretion was evidenced by denser collagen fibers. Besides, greater ingrowth of collagen into scaffolds, as expressed as wider overlap compared with the PLGA group, indicated better biocompatibility.[40]

Better biocompatibility leads to better biomechanical performance. Higher maximum failure load of the regenerated tendon was noticed on the PLGA/Col scaffold rather than on the PLGA scaffold or the normal sample. In both groups, the cross-sectional area increased over time and was significantly larger than the normal value, which was a result of cell recruitment and adhesion. We noticed that cells seeded on the PLGA nano-scaffold showed inferior biocompatibility to the tissue culture plate *in vitro*. This may be a consequence of the hydrophobic property of this material, to which the ability of cells to adhere was limited, and this therefore restricted cell proliferation during early stages. Despite the limited effect of the PLGA scaffold on cell attachment *in vitro*, the scaffold *in vivo* was surrounded by adjacent tissue and body fluid, and consequently may improve the biocompatibility.[20] However, the ultimate stress in the PLGA/Col group was significantly higher than that in the PLGA group. This illustrated that the quality of the regenerated tendon was higher in the PLGA/Col group.

Hydroxyapatite (HA) is a primary component in natural bone with excellent osteoinductivity and biocompatibility.[41] However, it is proven that HA is inferior to PCL for bone regeneration.[42] By simulating hydroxyapatite crystals in natural human bone tissues, nHA is believed to be superior to micro-sized hydroxyapatite materials regarding protein absorption and cell attachment.[15,43] Researchers have found that PCL/nHA supports the growth, osteogenesis gene expression, and osteogenic differentiations in different cell lines by enhancement of osteogenic gene expression and the activity of ALP.[25,31,44] In the early stages of mineralization, HA crystals deposit within the cells and then propagate into the extracellular matrix. ALP promotes mineralization by hydrolyzing pyrophosphates and providing inorganic phosphates. Therefore, ALP is a widely recognized marker of early osteoblast differentiation and osteogenic activity.[45] In this study, we found similar results. Osteoblasts had better ALP activity on PCL/nHA than on PCL *in vitro*, and this difference was further observed as a difference in the amount of newly formed bone in the bone tunnel *in vivo*, even if the scaffold integrated with the surrounding host bone so well that no sample was pulled out from the tunnel.

Our results supported the application of dual co-electrospun nano-scaffolds in bridging the defects of MRCTs. Previous articles used polyglycolic acid sheets or mesenchymal stem cell seeded sheets to bridge the MRCTs on the same model.[8,9] The greatest maximum failure load of the regenerated tendon was 91.8 N, with an ultimate stress of 3.04 MPa at 16 weeks after surgery.[9] This was lower than the data in the PLGA–PCL group in our study. Besides, the doping of Col and nHA at the tendon side and bone side, respectively, further strengthened the newly formed tendon and the scaffold-bone healing. Therefore a co-electrospun dual nano-scaffold of PLGA/Col-PCL/nHA is a promising treatment for MRCT.

There are several limitations in the current study. First, assessment of the entire surface of the culture plate through fluorescent microscopy was not performed, which could lead to sampling error due to irregular cell distribution. Second, in the middle part of the transitional patch, both PLGA or PLGA/Col and PCL or PCL/nHA took part in the formation, and it was impossible to make an analysis for this part because the ratio of both materials was uncertain. Finally, the rotator cuff tear model was relatively small with behavior different to humans, and the rotator cuff tear was an acute rather than a chronic model, which might undermine the results.

Conclusion

In this study, a dual co-electrospun nano-scaffold of PLGA–PCL is used to bridge the defects of MRCTs in rabbit models and is found to be effective in rotator cuff regeneration. The incorporation of Col and nHA to PLGA and PCL, respectively, further enhances the biocompatibility and strengthens the reorganized tissue, and is therefore promising in the repair of MRCTs.

Conflict of interest

None.

Published on 14 October 2016. Downloaded by Boston University on 06/11/2016 08:01:31.

Acknowledgements

This study was supported by the National Natural Science Foundation of China (No. 81472142), the National Basic Research Program of China (2014CB964600 and 2012CB966300) and the National Natural Science Foundation of China (81271369).

References

1 G. Merolla, *et al.*, Tendon transfer for irreparable rotator cuff tears: indications and surgical rationale, *Muscles Ligaments Tendons J.*, 2014, **4**(4), 425–432.
2 R. H. Cofield, Subscapular muscle transposition for repair of chronic rotator cuff tears, *Surg., Gynecol. Obstet.*, 1982, **154**(5), 667–672.
3 C. Gerber, B. Fuchs and J. Hodler, The results of repair of massive tears of the rotator cuff, *J. Bone Jt. Surg., Am. Vol.*, 2000, **82**(4), 505–515.
4 A. Bedi, *et al.*, Massive tears of the rotator cuff, *J. Bone Jt. Surg., Am. Vol.*, 2010, **92**(9), 1894–1908.
5 M. Petri, *et al.*, Patch-Augmented Latissimus Dorsi Transfer and Open Reduction-Internal Fixation of Unstable Os Acromiale for Irreparable Massive Posterosuperior Rotator Cuff Tear, *Arthrosc. Tech.*, 2015, **4**(5), e487–e492.
6 M. Flury, Patch augmentation of the rotator cuff: a reasonable choice or a waste of money?, *Orthopade*, 2016, **45**(2), 136–142.
7 D. Mori, *et al.*, Effect of fatty degeneration of the infraspinatus on the efficacy of arthroscopic patch autograft procedure for large to massive rotator cuff tears, *Am. J. Sports Med.*, 2015, **43**(5), 1108–1117.
8 S. Yokoya, *et al.*, Tendon-bone insertion repair and regeneration using polyglycolic acid sheet in the rabbit rotator cuff injury model, *Am. J. Sports Med.*, 2008, **36**(7), 1298–1309.
9 S. Yokoya, *et al.*, Rotator cuff regeneration using a bioabsorbable material with bone marrow-derived mesenchymal stem cells in a rabbit model, *Am. J. Sports Med.*, 2012, **40**(6), 1259–1268.
10 S. E. Kim, *et al.*, Electrospun gelatin/polyurethane blended nanofibers for wound healing, *Biomed. Mater.*, 2009, **4**(4), 044106.
11 Y. Fu, *et al.*, Human urine-derived stem cells in combination with polycaprolactone/gelatin nanofibrous membranes enhance wound healing by promoting angiogenesis, *J. Transl. Med.*, 2014, **12**(1), 274.
12 G. Coskun, *et al.*, Histological evaluation of wound healing performance of electrospun poly(vinyl alcohol)/sodium alginate as wound dressing *in vivo*, *Biomed. Mater. Eng.*, 2014, **24**(2), 1527–1536.
13 S. Sahoo, S. L. Toh and J. C. Goh, A bFGF-releasing silk/PLGA-based biohybrid scaffold for ligament/tendon tissue engineering using mesenchymal progenitor cells, *Biomaterials*, 2010, **31**(11), 2990–2998.
14 W. Shen, *et al.*, Long-term effects of knitted silk-collagen sponge scaffold on anterior cruciate ligament reconstruction and osteoarthritis prevention, *Biomaterials*, 2014, **35**(28), 8154–8163.
15 F. Han, *et al.*, Hydroxyapatite-doped polycaprolactone nanofiber membrane improves tendon–bone interface healing for anterior cruciate ligament reconstruction, *Int. J. Nanomed.*, 2015, **10**, 7333–7343.
16 W. Zhang, *et al.*, *In vivo* evaluation of two types of bioactive scaffold used for tendon–bone interface healing in the reconstruction of anterior cruciate ligament, *Biotechnol. Lett.*, 2011, **33**(4), 837–844.
17 Q. Yao, *et al.*, Design, construction and mechanical testing of digital 3D anatomical data-based PCL-HA bone tissue engineering scaffold, *J. Mater. Sci.: Mater. Med.*, 2015, **26**(1), 5360.
18 S. Sahoo, S. L. Toh and J. C. Goh, PLGA nanofiber-coated silk microfibrous scaffold for connective tissue engineering, *J. Biomed. Mater. Res., Part B*, 2010, **95**(1), 19–28.
19 W. Zhang, *et al.*, Weft-knitted silk-poly(lactide-*co*-glycolide) mesh scaffold combined with collagen matrix and seeded with mesenchymal stem cells for rabbit Achilles tendon repair, *Connect. Tissue Res.*, 2015, **56**(1), 25–34.
20 S. Zhao, *et al.*, Biological augmentation of rotator cuff repair using bFGF-loaded electrospun poly(lactide-*co*-glycolide) fibrous membranes, *Int. J. Nanomed.*, 2014, **9**, 2373–2385.
21 P. Bhattacharjee, *et al.*, Non-mulberry silk fibroin grafted poly(capital JE, Ukrainian-caprolactone)/nano hydroxyapatite nanofibrous scaffold for dual growth factor delivery to promote bone regeneration, *J. Colloid Interface Sci.*, 2016, **472**, 16–33.
22 X. Gao, *et al.*, Polydopamine-templated hydroxyapatite reinforced polycaprolactone composite nanofibers with enhanced cytocompatibility and osteogenesis for bone tissue engineering, *ACS Appl. Mater. Interfaces*, 2016, **8**(5), 3499–3515.
23 R. Nithya and N. Meenakshi Sundaram, Biodegradation and cytotoxicity of ciprofloxacin-loaded hydroxyapatite-polycaprolactone nanocomposite film for sustainable bone implants, *Int. J. Nanomed.*, 2015, **10**(suppl 1), 119–127.
24 L. Weng, *et al.*, Highly controlled coating of strontium-doped hydroxyapatite on electrospun poly(varepsilon-caprolactone) fibers, *J. Biomed. Mater. Res., Part B*, 2016, DOI: 10.1002/jbm.b.33598.
25 J. P. Chen and Y. S. Chang, Preparation and characterization of composite nanofibers of polycaprolactone and nanohydroxyapatite for osteogenic differentiation of mesenchymal stem cells, *Colloids Surf., B*, 2011, **86**(1), 169–175.
26 J. Wang, *et al.*, Collagen/silk fibroin composite scaffold incorporated with PLGA microsphere for cartilage repair, *Mater. Sci. Eng., C*, 2016, **61**, 705–711.
27 J. C. Gayton, *et al.*, Rabbit supraspinatus motor endplates are unaffected by a rotator cuff tear, *J. Orthop. Res.*, 2013, **31**(1), 99–104.
28 A. Inui, *et al.*, Regeneration of rotator cuff tear using electrospun poly(D,L-lactide-*co*-glycolide) scaffolds in a rabbit model, *Arthroscopy*, 2012, **28**(12), 1790–1799.
29 M. R. Ladd, *et al.*, Co-electrospun dual scaffolding system with potential for muscle-tendon junction tissue engineering, *Biomaterials*, 2011, **32**(6), 1549–1559.
30 J. Xie, *et al.*, Osteogenic differentiation and bone regeneration of iPSC-MSCs supported by a biomimetic nanofibrous scaffold, *Acta Biomater.*, 2016, **29**, 365–379.

 This journal is © The Royal Society of Chemistry 2016

Published on 14 October 2016. Downloaded by Boston University on 06/11/2016 08:01:31.

31 M. J. Ban, *et al.*, The Efficacy of Fibroblast Growth Factor for the Treatment of Chronic Vocal Fold Scarring: From Animal Model to Clinical Application, *Clin. Exp. Otorhinolaryngol.*, 2016, DOI: 10.21053/ceo.2016.00941.

32 P. Ciampi, *et al.*, The benefit of synthetic versus biological patch augmentation in the repair of posterosuperior massive rotator cuff tears: a 3-year follow-up study, *Am. J. Sports Med.*, 2014, **42**(5), 1169–1175.

33 T. Mihata, *et al.*, Superior capsule reconstruction to restore superior stability in irreparable rotator cuff tears: a biomechanical cadaveric study, *Am. J. Sports Med.*, 2012, **40**(10), 2248–2255.

34 B. A. Lenart, *et al.*, Treatment of massive and recurrent rotator cuff tears augmented with a poly-L-lactide graft, a preliminary study, *J. Shoulder Elb. Surg.*, 2015, **24**(6), 915–921.

35 Z. Rezvani, *et al.*, A bird's eye view on the use of electrospun nanofibrous scaffolds for bone tissue engineering: current state-of-the-art, emerging directions and future trends, *Nanomedicine*, 2016, **12**(7), 2181–2200.

36 D. P. Beason, *et al.*, Fiber-aligned polymer scaffolds for rotator cuff repair in a rat model, *J. Shoulder Elb. Surg.*, 2012, **21**(2), 245–250.

37 S. Zhao, *et al.*, Healing improvement after rotator cuff repair using gelatin-grafted poly(L-lactide) electrospun fibrous membranes, *J. Surg. Res.*, 2015, **193**(1), 33–42.

38 S. Samavedi, *et al.*, Response of bone marrow stromal cells to graded co-electrospun scaffolds and its implications for engineering the ligament–bone interface, *Biomaterials*, 2012, **33**(31), 7727–7735.

39 P. Zhang, *et al.*, Local delivery of controlled-release simvastatin to improve the biocompatibility of polyethylene terephthalate artificial ligaments for reconstruction of the anterior cruciate ligament, *Int. J. Nanomed.*, 2016, **11**, 465–478.

40 M. M. Zimkowski, *et al.*, Biocompatibility and tissue integration of a novel shape memory surgical mesh for ventral hernia: *in vivo* animal studies, *J. Biomed. Mater. Res., Part B*, 2014, **102**(5), 1093–1100.

41 R. Z. LeGeros, Properties of osteoconductive biomaterials: calcium phosphates, *Clin. Orthop. Relat. Res.*, 2002, **395**, 81–98.

42 H. Eftekhari, *et al.*, Assessment of polycaprolactone (PCL) nanocomposite scaffold compared with hydroxyapatite (HA) on healing of segmental femur bone defect in rabbits, *Artif. Cells, Nanomed., Biotechnol.*, 2016, 1–8.

43 G. Wei and P. X. Ma, Structure and properties of nano-hydroxyapatite/polymer composite scaffolds for bone tissue engineering, *Biomaterials*, 2004, **25**(19), 4749–4757.

44 B. Chuenjitkuntaworn, *et al.*, The efficacy of polycaprolactone/hydroxyapatite scaffold in combination with mesenchymal stem cells for bone tissue engineering, *J. Biomed. Mater. Res., Part A*, 2016, **104**(1), 264–271.

45 H. Orimo, The mechanism of mineralization and the role of alkaline phosphatase in health and disease, *J. Nippon Med. Sch.*, 2010, **77**(1), 4–12.